ChemElectroChem

Research Article
doi.org/10.1002/celc.202201074

Chemistry Europe
European Chemical Societies Publishing

www.chemelectrochem.org

Special Collection

Stable Cycling of Sodium Metal Anodes Enabled by a Sodium/Silica-Gel Host

Angelica Petrongari,[a] Mariarosaria Tuccillo,[a] Andrea Ciccioli,[a] Alessandro Latini,[a] and Sergio Brutti*[a, b, c]

Sodium metal batteries (SMBs) are innovative and promising energy storage systems. SMBs are a competitive technological paradigm compared to the state-of-the-art lithium-ion batteries thanks to the high specific capacity of sodium metal, i.e., 1166 mAh g^{-1}, and the Na^+/Na^0 low redox potential of −2.71 V vs. standard hydrogen electrode. Unstable solid electrolyte interface (SEI), uncontrolled overpotentials and dendrite growth of sodium are the main drawbacks that hinder the development of SMBs. Herein, we propose a functionalized silica gel material with extended porosity (NaSGII) as an active host material in order to obtain stable cycling of sodium metal anodes. NaSGII was incorporated in composite electrodes using a conductive carbon additive and polymeric binders and the functional properties in SMBs cells demonstrated by galvanostatic tests. A Butler-Volmer analysis demonstrated an improvement of electrokinetic parameters induced by NaSGII.

Introduction

The increasing demand of energy storage systems requires further efforts to improve the performances of secondary batteries beyond the current state-of-the-art. In this respect, Na-based batteries are becoming a realistic alternative to Li-ion systems, despite their poorer gravimetric performance.

On the other hand, metallic sodium has been targeted as a promising anode material owing to its high theoretical capacity of 1166 mAh g^{-1} and low redox potential of −2.71 V vs. standard hydrogen electrode (SHE).[1,2] Its use as an anode in sodium batteries may open the way towards next generation of Na-batteries, including high energy density systems such as Na–S (1274 Wh kg^{-1})[3] and Na-O_2 (1108 Wh kg^{-1})[4] batteries, with theoretical features comparable to lithium-ion cells.

However, the optimization of reversible Na metal anodes faces significant hurdles, like uneven nucleation, dendrite growth and solid electrolyte interface (SEI) instability,[5,6] The dendritic growth of Na metal upon plating is a serious problem, as it may origin internal short circuit leading to cell failure and possible electrolyte ignition.[7] Nevertheless, cell failure may also occur due to uncontrolled SEI growth, leading to electrolyte depletion and increasing overpotentials.[8] Thereby, multiple research strategies are required to improve the reversibility of sodium plating/stripping, thus disclosing reliable sodium metal electrodes, able to outperform current hard carbon benchmarks.

In order to control the reversibility of Na electrodeposition, many studies focus on the stabilization of the SEI by the optimization of the liquid electrolyte formulation[9] or by tailored artificial SEIs.[10] Solid-state electrolytes are also taken into account as they can offer a mechanical resistance to dendrite growth.[11,12]

Recently, the use of porous current collectors,[13,14] or composite electrode surfaces has been demonstrated as valuable and successful strategy. Wang et al. designed anodes made by Au nanoparticles supported on a reduced graphene oxide scaffold, showing excellent coulombic efficiencies and a dendrite-free deposition morphology of sodium.[15] These results demonstrate that highly porous hosts allow a homogenous metallic sodium plating and prevent detrimental phenomena like concentration polarization and dendrite growth.

Herein we demonstrate the use of a sodium silica gel-based composite electrode (NaSGII) as a host material for reversible sodium metal electrodeposition for the first time in the literature. NaSGII is currently used as reducing agent for the hydrogen production and it is obtained by absorption of liquid Na into nanostructured silica gel at 400 °C for 15 h.[16,17] Overall, NaSGII is a composite nanocrystalline material constituted by Na_4Si_4 and Na_2SiO_3[16] with narrow mesopores in the nominal range of 10–30 nm and a surface area of hundreds of square meters per gram.[17] Sodium silicide is the most sodiophilic component because of its reactivity as reducing agent, so its role in the sodium metal anode is to provide a large number of

[a] A. Petrongari, M. Tuccillo, Dr. A. Ciccioli, Prof. A. Latini, Prof. S. Brutti
Department of Chemistry
Sapienza University of Rome
P.le Aldo Moro 5, Rome, 00185, Italy
E-mail: sergio.brutti@uniroma1.it
Homepage: https://www.chem.uniroma1.it/dipartimento/persone/sergio-brutti
[b] Prof. S. Brutti
CNR-ISC, Consiglio Nazionale Delle Ricerche
Istituto Dei Sistemi Complessi
Rome, 00185, Italy
[c] Prof. S. Brutti
GISEL - Centro di Riferimento Nazionale per i Sistemi di Accumulo Elettrochimico di Energia
Florence, 50121, Italy

Supporting information for this article is available on the WWW under https://doi.org/10.1002/celc.202201074

An invited contribution to a Special Collection dedicated to Giornate dell'Elettrochimica Italiana 2022 (GEI2022)

nucleation sites for sodium metal deposition. Sodium silicate, on the other hand, is the main constituent (silicate:silicide ratio 5:1[16]) of the porous scaffold of NaSGII that ensures an even morphology of deposits. This features, along with the large surface area, are the key for achieving a reversible sodium metal plating/stripping.

Going beyond the demonstration of NaSGII in Na-metal batteries, in this study we tested electrode formulations with different binders: namely polyvinylidenfluoride (PVDF) and polyethylene oxide (PEO). These two common polymeric binders have significantly different physical properties: our aim is to evaluate the impact of the mechanical properties of the binder on the electrochemical performance of NaSGII-based electrodes in Na metal batteries.

Overall, tests performed on half cells NaSGII-SP-PEO||Na or NaSGII-SP-PVDF||Na demonstrate a ~100% columbic efficiency (CE) for 200 cycles of plating/stripping with very small overpotentials. Apparently, the alteration of the electrokinetic parameters estimated by a Butler-Volmer analysis confirms that NaSGII tunes the kinetics of sodium plating/stripping compared to flat Al electrodes enhancing the electrochemical reversibility.

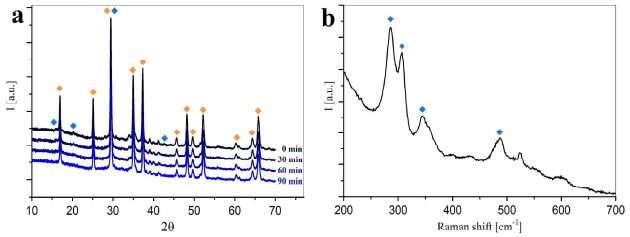

Figure 1. a) XRD spectrum of Na-SG-II. Orange labels refer to Na_2SiO_3 phase, blue labels refer to Na_4Si_4 phase. b) Raman spectrum of Na-SG-II. Blue labels refer to Na_4Si_4 vibrations.

Results and Discussion

Characterization of the NaSGII and pristine electrodes

The Na-SG-II nanocrystalline pristine material has been analyzed by XRD and Raman spectra (Figure 1). The XRD pattern (Figure 1a) shows mainly the Na_2SiO_3 phase:[18] only minor reflections due to Na_4Si_4 are observed.[19] As expected,[16,17] Na metal XRD fingerprints are missing in the pristine material. The XRD spectrum registered after 2 h of air exposure of Na-SG-II shows the disappearance of Na_4Si_4 reflections: this is a clue of the reactivity of NaSGII with moisture, likely due to the reaction $2NaSi + 5H_2O \rightarrow Na_2Si_2O_5$. The Raman spectrum of NaSGII registered in a strictly anhydrous confined sample holder shows the typical signals[20] of Si_4^{4-} unit at 280 cm^{-1}, 305 cm^{-1}, 350–380 cm^{-1} and 487 cm^{-1} (Figure 1b).

Overall, Na_2SiO_3 and Na_4Si_4 are the main constituents of the pristine Na-SG-II material and the reactivity with air moisture requires a careful handling of this material in anhydrous environment.

All manufactured electrodes have been analyzed by SEM to evaluate the surface morphologies.

Benchmark SP-PEO and SP-PVDF electrodes (Figures 2a and 2d) show the typical homogeneous morphology of carbon black coatings. On the other hand, NaSGII-SP-PEO and NaSGII-SP-PVDF samples (Figures 2b and 2e) show also a homogeneous distribution of the active material within the carbon black coating. The estimate of the mean diameter of NaSGII particles has been carried out by a digital analysis of SEM micrographs using the ImageJ software:[21] particle shapes have been approximated to spheres. In both NaSGII-containing samples the mean grain size of NaSGII was 1.7 μm with a similar size distribution, as reported in the Figures 2c and 2f.

Overall electrodes manufactured using PEO or PVDF show very similar pristine morphologies and analogue dispersions of the NaSGII material despite the different polymer binders.

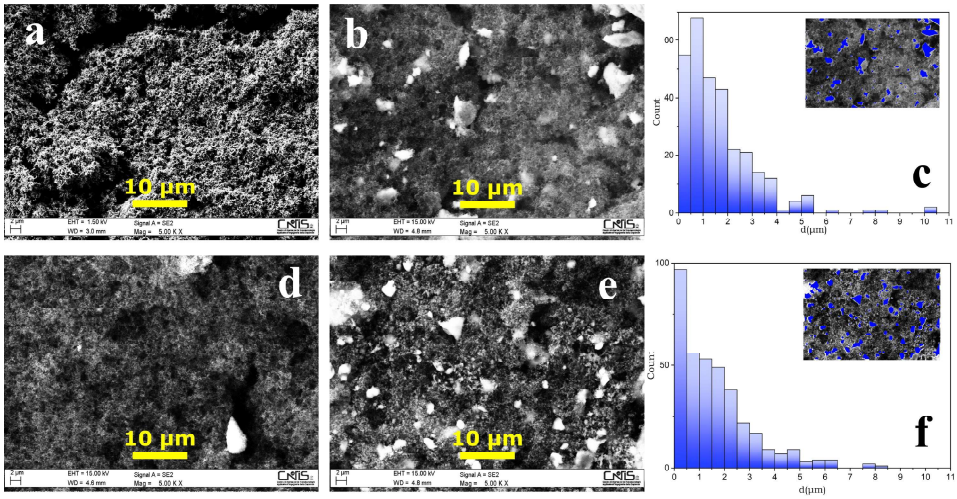

Figure 2. SEM images at 5.000x magnification of a) SP-PVDF, b) NaSGII-SP-PVDF, d) SP-PEO and e) NaSGII-SP-PEO. c) Grain size distribution of NaSGII in NaSGII-SP-PVDF samples. f) Grain size distribution of NaSGII in NaSGII-SP-PEO samples.

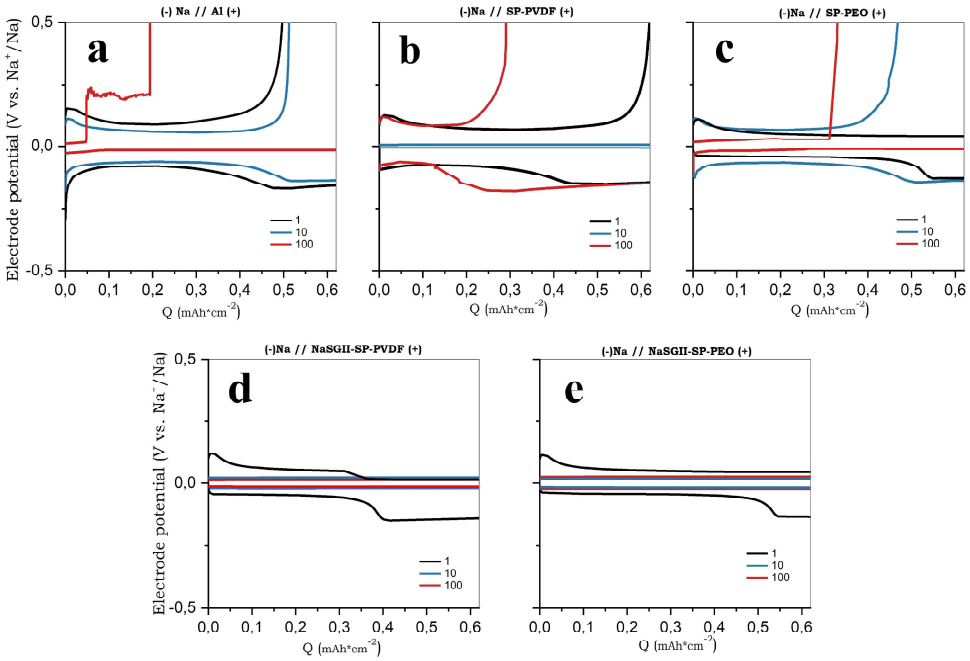

Figure 3. Potential-capacity profiles of working electrodes: a) uncoated Al, b) SP-PVDF, c) SP-PEO, d) NaSGII-SP-PVDF, e) NaSGII-SP-PEO. NaTFSI 1 M in PC + 3% FEC electrolyte was used.

Electrochemical performance

The reversibility of the electrochemical Na plating/stripping has been evaluated by performing galvanostatic tests at 0.6 mA cm^{-2} with a capacity limitation of 0.6 mAh·cm^{-2} (Figure 3). Upon discharge (plating) all sodium-less electrodes, either containing the NaSGII active material or without, show potential profiles with similar shapes in the 1st cycle, where the formation of the SEI occurs. However, all benchmark samples (Figure 3a–c) show abrupt changes in the first cycle discharge/charge profiles, also seen in subsequent cycles, indicating an uneven reactivity between sodium metal and the electrolyte and the possible sudden break of the SEI. A different picture occurs upon charge, in the stripping step of the galvanostatic tests. All benchmark samples, i.e., Al, SP-PVDF and SP-PEO, show abrupt increases in the electrode potentials and fail before reaching a fully reversible Na-stripping. This leads to poor efficiency of sodium plating/stripping, particularly in the case of uncoated Al (Figure 3a) and SP-PEO (Figure 3b). Upon cycling all benchmark electrodes show poor and scattered reversibility, as shown in the Figure 4a, whereas the incorporation of NaSGII (Figure 3d and 3e) in the porous electrode leads to small overpotentials upon cycling, full reversibility of the Na plating/stripping (Figure 4b) and almost negligible deterioration of the electrochemical performance for 200 cycles. Overall, the use of NaSGII drastically improves the reversibility of Na plating/stripping.

Having established the superior performance of NaSGII-based composite porous electrodes additional tests have been carried out in order to record the performance at increasing current rates (Figure 4c, 4e) and increasing capacity limits as shown in the Figure 4d and 4f. Apart from limited coulombic inefficiencies at 0.1 mA cm^{-2} small current rate, the NaSGII-PVDF electrodes are able to deliver a full reversibility of Na stripping/plating in all experimental conditions. An even better picture is observed in the case of NaSGII-PEO electrodes, where a 100% CE is obtained at all current densities and for all the capacity limits. Remarkably an excellent reversibility is observed at 1 mAh cm^{-2} at 0.6 mA cm^{-2} using both polymer binders.

In order to shed light on the origin of the enhancement of the performance, we carried out chronopotentiometry tests to estimate the Butler-Volmer (B-V) parameters and compare the plating/stripping electrokinetics on the different electrodes. The corresponding Tafel plots reporting the chronopotentiometry results for all materials are shown in the Figure 5. Kinetic parameters obtained for each sample by a B-V fitting are summarized in Table 1. As expected, the sodium metal plating/stripping on uncoated aluminum is strongly asymmetric, as demonstrated by the extremely small anodic symmetry factor (β) value of 0.02. This implies a kinetically unfavoured electrochemical dissolution of metallic sodium. Conversely, both benchmarks and NaSGII-containing electrodes show an opposite behaviour, since all β values above 0.5 suggest kinetic hinderance of the sodium plating. These results are in line with β values for sodium electroplating previously reported in

Table 1. Values of exchange current density J_0 and symmetry factor β obtained from the fit of experimental data as represented in Figure 5.

	Uncoated Al	SP-PVDF	NaSGII-SP-PVDF	SP-PEO	NaSGII-SP-PEO
J_0 [mA cm^{-2}]	0.700	0.035	0.052	0.084	0.104
β	0.02	0.63	0.69	0.65	0.67

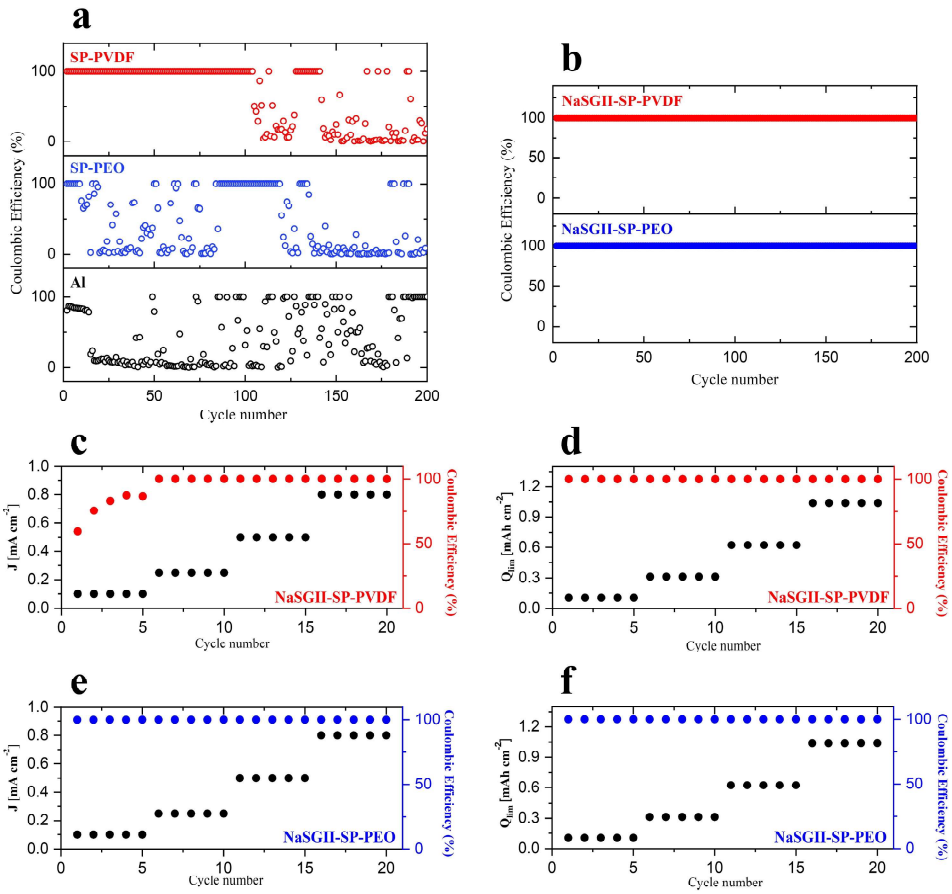

Figure 4. a) Coulombic efficiencies of benchmark samples SP-PVDF, SP-PEO and uncoated Al cycled at $J = 0.6\ mA\,cm^{-2}$, $Q_{lim} = 0.6\ mAh\,cm^{-2}$. b) Coulombic efficiencies of NaSGII-containing samples cycled at $J = 0.6\ mA\,cm^{-2}$, $Q_{lim} = 0.6\ mAh\,cm^{-2}$. c) Coulombic efficiencies of NaSGII-SP-PVDF sample cycled with a capacity limit of $0.6\ mAh\,cm^{-2}$ and increasing current rates 0.1, 0.25, 0.5 and $0.8\ mA\,cm^{-2}$. d) Coulombic efficiencies of NaSGII-SP-PVDF cycled with $J = 0.6\ mA\,cm^{-2}$ and increasing capacity limits 0.1, 0.3, 0.6, $1\ mAh\,cm^{-2}$. e) Coulombic efficiencies of NaSGII-SP-PEO sample cycled with a capacity limit of $0.6\ mAh\,cm^{-2}$ and increasing current rates of 0.1, 0.25, 0.5 and $0.8\ mA\,cm^{-2}$. f) Coulombic efficiencies of NaSGII-SP-PEO cycled with $J = 0.6\ mA\,cm^{-2}$ and increasing capacity limits 0.1, 0.3, 0.6, $1\ mAh\,cm^{-2}$.

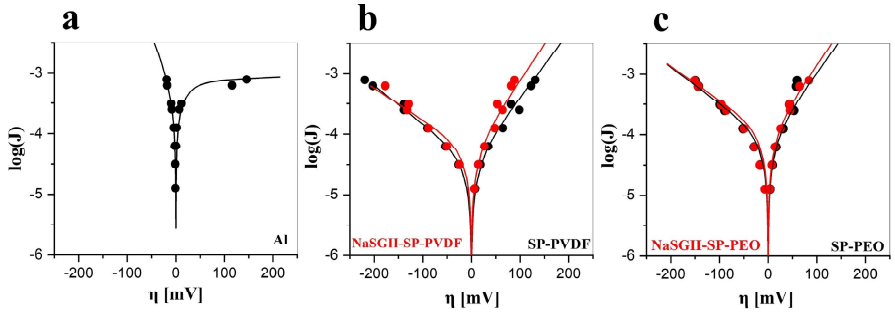

Figure 5. Butler-Volmer profiles of a) uncoated Al, b) SP-PVDF and NaSGII-SP-PVDF, c) SP-PEO and NaSGII-SP-PEO.

literature.[22] Overall, all exchange current densities (J_0) of coated electrodes (benchmarks and NaSGII-based) are smaller than bare aluminum.

The use of NaSGII has a limited impact on the symmetry factor comparing to the benchmarks but improves remarkably J_0 in respect to the SP-binder porous electrodes. Increases of J_0 of almost +24% and +48% are observed for PEO and PVDF based electrodes, respectively, which implies a remarkably faster electron transfer process. On passing it is important to recall that a moderate exchange current density is generally considered a requirement for homogeneous plating in the case of lithium:[23] it is likely that a similar mechanism occur also for sodium deposition. In this respect NaSGII seem to provide an optimal J_0 compared to composite benchmarks, thanks to a moderate growth/dissolution reaction rate, thus improving the uniformity of Na electrodeposition in respect to the case of the uncoated Al foil. Overall, our data suggest that a moderate deposition kinetics (J_0) coupled with a favourable stripping (β) is

the key for the excellent reversibility observed using NaSGII-based electrodes. In terms of kinetic parameters NaSGII-SP-PEO outperforms NaSGII-SP-PVDF having β slightly closer to 0.5 and a 2 times larger J_0.

Post-mortem characterization

SEM micrographs of NaSGII-SP-PVDF and NaSGII-SP-PEO electrodes after 200 cycles show evidence of significant differences between the SEI layers and electrode morphology depending on the binder used. Apparently PVDF-based electrodes (Figure 6a) promote the formation of a thick SEI on the electrode surface. The homogeneous and matching distributions of Na and F observed by EDX mapping (Figure 6c and S1) suggests the possible formation of NaF as main constituent of the SEI layer. An XPS validation of this evidence is necessary but unfortunately beyond our capabilities The presence of NaF is frequently observed in SMBs when salts containing fluorine are used;[24,25] moreover, NaF formation is favored for the use of fluoroethylene carbonate (FEC) as additive in the electrolyte.[26] This hypothesis is supported by the presence of extended cracks on the SEI as NaF stiffness (shear modulus of 31.4 MPa[5]) may easily lead to poor mechanical elasticity and poor volume buffering during cycling. One should recall that NaF role in the SEI of sodium metal anodes is controversial since it affects the mechanical stability of the interface but, at the same time, it is able to limit sodium dendrites growth.[27] In line with this expectation, post mortem NaSGII-SP-PVDF electrodes do not show evidence of dendrites. On the contrary, dendrites are observed in the case of NaSGII-SP-PEO over the surface of post mortem electrodes (see Figure 6b). Furthermore, dendrites are apparently not embedded in an organic or composite matrix, thus suggesting the formation of a very thin SEI. The small amounts of fluorine detected by EDX mapping of NaSGII-SP-PEO electrodes poorly correlate with sodium maps, hinting that the NaF content is significantly smaller than in the case of PVDF-based electrodes (Figure 6d). Moving to the cross-section images, electrode morphologies for samples NaSGII-SP-PVDF (Figure 6a) and NaSGII-SP-PEO (Figure 6b) resemble the morphologies of the respective surfaces. Electrode material and sodium deposits are surrounded by a thick layer when PVDF is used, while a more homogeneous morphology of sodium deposits without a thick surrounding layer is observed in the

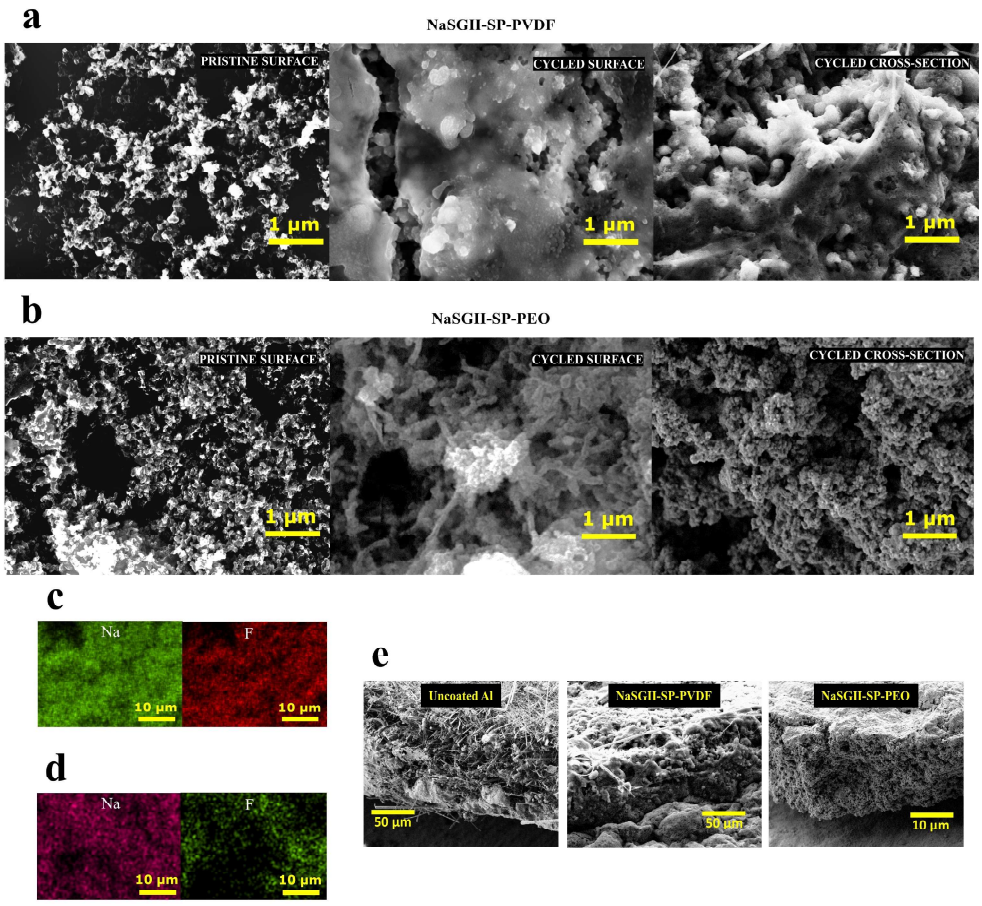

Figure 6. a) SEM images of pristine surface, cycled surface (200 cy) and cycled cross section (15 cy) of NaSGII-SP-PVDF with a 50.000x magnification. b) SEM image of pristine surface, cycled surface (200 cy) and cycled cross-section (15 cy) of NaSGII-SP-PEO with a 50.000x magnification. c) Sodium and fluorine elemental mapping on the surface of cycled NaSGII-SP-PVDF with a 5.000x magnification. d) Sodium and fluorine elemental mapping on the surface of cycled NaSGII-SP-PEO with a 5.000x magnification. e) Cross-section SEM images of uncoated Al (1.000x magnification), NaSGII-SP-PVDF (1.000× magnification) and NaSGII-SP-PEO (5.000x magnification).

case of NaSGII-SP-PEO. Sodium dendrites observed on the surface of the PEO-based electrode are missing in the cross-section, suggesting that dendritic growth is limited to the superficial layer. Overall, the use of PEO promotes a thin SEI unable to provide mechanical barriers to dendrites, likely rich in organic components. On the other hand, this SEI is apparently able to limit remarkably the accumulation of by-products over the surface of electrodes upon the Na stripping/deposition.

A macroscopic overview of electrode cross section for uncoated Al, NaSGII-SP-PVDF and NaSGII-SP-PEO after 15 cycles is displayed in Figure 6e. It is shown that sodium deposits on aluminum are detached from the support, and they are found into the separator fibers, indicating the formation of dead Na which is no more in electrical contact with the electrode. Separator fibers are observed also in the upper layer of the electrode NaSGII-SP-PVDF: this may be explained by the thick SEI, confirmed by all SEM micrographs related to this sample, which grows incorporating some of them. We speculate that this is not a clue of dead Na accumulation since Na deposition occurs under the SEI layer. In fact, no separator fibers nor evidence of dead Na are found in the case of the PEO-based sample.

A representative characterization of thickness evolution for the sample NaSGII-SP-PVDF is reported in Figure S2, showing negligible thickness changes after 15 cycles.

XPS measurements are necessary to further consolidate the composition of SEI formed upon cycling in both electrode formations since our evaluation basing on EDX mapping is at a qualitative level. Unfortunately, this experimental approach is currently beyond our capabilities.

Conclusion

This study demonstrate that NaSGII can be a suitable host material for Na-metal anodes in aprotic batteries, as it enables excellent reversibility of sodium plating/stripping and stable performance for almost 200 cycles. NaSGII improves the electrokinetics of sodium electrodeposition in both the electrode formulations here proposed: namely NaSGII-SP-PVDF and NaSGII-SP-PEO. The nature of the binder impacts the performance likely due to changes in the composition of the SEI layer, as qualitatively observed in the post-mortem SEM/EDX characterization of electrodes after 200 cycles. A thick and NaF-rich SEI is observed in the case of PVDF-based electrodes in which dendrite morphologies are missing. On the other hand, a thin and soft SEI forms in PEO-based electrodes that are to some extent affected by dendrite growth. The alteration of the SEI impacts remarkably on the Butler-Volmer parameters, since the NaSGII-SP-PEO electrode shows significantly higher exchange current densities (0.104 mA cm^{-2}) compared to the PVDF-based one (0.052 mA cm^{-2}). Further studies are required to consolidate this innovation and to extend the performance validation to higher current densities and capacity limits with the aim of verifying NaSGII stability in strict cycling conditions, that are mandatory for practical applications. These studies are in progress and will be reported elsewhere in the near future.

Experimental Section

Electrodes preparation

Sodium silica gel Stage II, fuel cell grade, was purchased from Sigma Aldrich. Mixtures of Na-SG-II, carbon black and polyvinylidenfluoride (PVDF) or polyethylene oxide (PEO, 750 kDa) were prepared at weight ratio of 80:15:5. The mixtures were added to THF at weight ratio of 2:100 and 80 μL of the as-prepared slurry were drop-casted in pre-cut aluminum discs with a 12.7 mm diameter. Al can be used as current collector in sodium metal batteries since it doesn't alloy with Na, and it is preferred to Cu for its lighter weight and lower cost.[28] Electrodes were dried in vacuum at 90 °C for 15 h. Besides the Na-SG-II electrodes also benchmark materials have been manufactured and tested. A summary of the samples, compositions and coding is reported in the Table 2.

Physical-chemical characterization

Each analysis was carried out keeping samples in air-confined environments to avoid reactions with moisture. Post mortem electrodes were washed twice in fresh dimethyl carbonate and tetrahydrofuran, then dried in vacuum. An HR-FESEM Zeiss Auriga coupled with a Bruker EDX system was used for morphological characterization. Raman spectra were acquired with a DILOR LabRam confocal micro-Raman with a He–Ne laser source at 632.7 nm, using a designed sample holder sealed under dried Ar and equipped with a glass window to allow sample protection and the spectroscopic investigation. XRD spectra were registered with a powder diffractometer Philips X'Pert Pro with a Cu K_α source at $\lambda =$ 1,54 Å. Samples have been sealed under a Kapton foil to preserve them from the interaction with moisture during the XRD run.

Electrochemical characterization

Electrochemical cells were assembled in an Ar filled glove box (Iteco Eng SGS-30, H_2O < 0.1 ppm), at room temperature. 1 M NaTFSI (sodium bis(trifluoromethyl sulphonyl) imide) in PC (propyelene carbonate) +3% FEC electrolyte and Whatman ® glass fiber separators were used. ECC-Std test cells have been used (EL-Cell).

Before any electrochemical test, an activation procedure was applied to electrodes, consisting in a chronopotentiometry run at increasing negative currents: −0.04 mA (600 s); −0.079 mA (300 s); −0.158 mA (150 s); −0.237 mA (100 s); −0.316 mA (75 s); −0.395 mA (60 s); −0.592 mA (40 s); −0.790 mA (30 s); −0.988 mA (24 s); −1.580 mA (7.5 s), −2.370 mA (5 s), −3.950 mA (3 s). Consid-

Table 2. Summary of samples prepared (ratios are expressed in unit weight).

Sample	Code	Slurry composition[a]	Electrode composition and mean loading[b]
Al	Al	Uncoated	Uncoated
Al coated with carbon black and PEO	SP-PEO	0.45:0.05:0:99.7	90:10 0.3–0.5 mg cm^{-2}
Al coated with carbon black and PVDF	SP-PVDF	1.8:0.2:0:98	90:10 1.0–1.5 mg cm^{-2}
Al coated with NaSGII, carbon black and PEO	NaSGII-SP-PEO	0.3:0.1:1.6:98	15:5:80 1.0–1.5 mg cm^{-2}
Al coated with NaSGII, carbon black and PVDF	NaSGII-SP-PVDF	0.3:0.1:1.6:98	15:5:80 1.0–1.5 mg cm^{-2}

[a] Carbon black:binder:NaSGII:THF. [b] Carbon black:binder:NaSGII.

ering the geometrical area of the electrodes ($s = 1.27\ cm^2$) the net effect of the activation procedure is to "pre-plate" 0.055 mAh cm^{-2} on the active material: this treatment is aimed at pre-form nucleation seeds for Na. Galvanostatic cycling tests were run on NaSGII-SP-PEO||Na and NaSGII-SP-PVDF||Na cells at 0.6 mA cm^{-2} with a limited capacity of 0.6 mAh cm^{-2} and a cut-off potential range between −1.5 and +1.5 vs. Na^+/Na^0.

Butler-Volmer analysis

Experimental runs were carried out by a chronopotentiometry run at different areal current densities ranging from ±0.013 to ±0.778 mA cm^{-2}. All the measurements were performed at 30 °C in a Memmert oven. The exchange current density J_0 and symmetry factor β were estimated by using a non-linear fitting of the observed overpotentials (η) in respect to the experimental current density (*J*), assuming the Butler-Volmer Equation (1):

$$J = J_0 \cdot \left[e^{(\beta F/RT)\cdot\eta} - e^{(-(1-\beta)F)/RT)\cdot\eta}\right] \quad (1)$$

Where R is the gas constant, F is the Faraday constant and T the temperation expressed in Kelvin. An in-house fitting algorithm was used for the non-linear regression of the experimental data.

Acknowledgements

The authors would like to acknowledge University of Rome La Sapienza for the support through the project ATENEO 2019 "CUTE - Confined nanometals: strUcture and properties of alkali meTals in mEsopores" and Italian Ministry of Economic Development in the frame of PNRR - CN4 (Centro Nazionale Mobilità Sostenibile) – Spoke 13 "Trazione elettrica e batterie".

Conflict of Interest

The authors declare no conflict of interest.

Data Availability Statement

The data that support the findings of this study are available from the corresponding author upon reasonable request.

Keywords: aprotic batteries · charge transfer · electrochemistry · secondary batteries · sodium batteries

Manuscript received: October 28, 2022
Revised manuscript received: December 23, 2022

[1] W. Luo, L. Hu, *ACS Cent. Sci.* **2015**, *1*, 420–422.
[2] P. Hartmann, C. L. Bender, M. Vračar, A. K. Dürr, A. Garsuch, J. Janek, P. Adelhelm, *Nat. Mater.* **2013**, *12*, 228–232.
[3] S. Zhang, Y. Yao, Y. Yu, *ACS Energy Lett.* **2021**, *6*, 529–536.
[4] Z. Zheng, C. Wu, Q. Gu, K. Konstantinov, J. Wang, *Energy Environ. Mater.* **2021**, *4*, 158–177.
[5] B. Lee, E. Paek, D. Mitlin, S. W. Lee, *Chem. Rev.* **2019**, *119*, 5416–5460.
[6] R. Mogensen, D. Brandell, R. Younesi, *ACS Energy Lett.* **2016**, *1*, 1173–1178.
[7] J. Yang, M. Zhang, Z. Chen, X. Du, S. Huang, B. Tang, T. Dong, H. Wu, Z. Yu, J. Zhang, G. Cui, *Nano Res.* **2019**, *12*, 2230–2237.
[8] A. Patrike, P. Yadav, V. Shelke, M. Shelke, *ChemSusChem* **2022**, *15*, e202200504.
[9] R. Jiang, L. Hong, Y. Liu, Y. Wang, S. Patel, X. Feng, H. Xiang, *Energy Storage Mater.* **2021**, *42*, 370–379.
[10] Q. Chen, H. He, Z. Hou, W. Zhuang, T. Zhang, Z. Sun, L. Huang, *J. Mater. Chem. A* **2020**, *8*, 16232–16237.
[11] L. Shen, S. Deng, R. Jiang, G. Liu, J. Yang, X. Yao, *Energy Storage Mater.* **2022**, *46*, 175–181.
[12] C. Simari, M. Tuccillo, S. Brutti, I. Nicotera, *Electrochim. Acta* **2022**, *410*, 139936.
[13] J. Sun, C. Guo, Y. Cai, J. Li, X. Sun, W. Shi, S. Ai, C. Chen, F. Jiang, *Electrochim. Acta* **2019**, *309*, 18–24.
[14] Q. Lu, X. Wang, A. Omar, D. Mikhailova, *Mater. Lett.* **2020**, *275*, 128206.
[15] H. Wang, T. Jiang, B. Wang, L. Zhang, D. Kong, T. Xu, J. Zang, Z. Zhang, X. Li, Y. Wang, *J. Power Sources* **2021**, *507*, 230294.
[16] M. Shatnawi, G. Paglia, J. L. Dye, K. C. Cram, M. Lefenfeld, S. J. L. Billinge, *J. Am. Chem. Soc.* **2007**, *129*, 1386–1392.
[17] J. L. Dye, P. Nandi, J. E. Jackson, M. Lefenfeld, P. A. Bentley, B. M. Dunyak, F. E. Kwarcinski, C. M. Spencer, T. N. Lindman, P. Lambert, P. K. Jacobson, M. Y. Redko, *Chem. Mater.* **2011**, *23*, 2388–2397.
[18] A. Grund, M. Pizy, *Acta Crystallogr.* **1952**, *5*, 837.
[19] T. Goebel, Y. Prots, F. Haarmann, *Z. Kristallogr. New Cryst. Struct.* **2008**, *223*, 187–188.
[20] K. Annou, M. Pelosi, G. Gershinsky, F. Favier, Y. Cuminal, M. Tillard, D. Zitoun, *Mater. Renew. Sustain. Energy* **2021**, *3*, 32.
[21] C. A. Schneider, W. S. Rasband, K. W. Eliceiri, *Nat. Methods* **2012**, *97*, 671–675.
[22] R. Wibowo, L. Aldous, E. I. Rogers, S. E. Ward Jones, R. G. Compton, *J. Phys. Chem. C* **2010**, *114*, 3618–3626.
[23] Y. Liu, X. Xu, M. Sadd, O. O. Kapitanova, V. A. Krivchenko, J. Ban, J. Wang, X. Jiao, Z. Song, J. Song, S. Xiong, A. Matic, *Adv. Sci.* **2021**, *8*, 2003301.
[24] Y. Lee, J. Lee, J. Lee, K. Kim, A. Cha, S. Kang, T. Wi, S. J. Kang, H. W. Lee, N. S. Choi, *ACS Appl. Mater. Interfaces* **2018**, *10*, 15270–15280.
[25] S. Wang, Y. Chen, Y. Jie, S. Lang, J. Song, Z. Lei, S. Wang, X. Ren, D. Wang, X. Li, R. Cao, G. Zhang, S. Jiao, *Small Methods* **2020**, *4*, 1900856.
[26] R. Rodriguez, K. E. Loeffler, S. S. Nathan, J. K. Sheavly, A. Dolocan, A. Heller, C. B. Mullins, *ACS Energy Lett.* **2017**, *2*, 2051–2057.
[27] Z. Wei Seh, J. Sun, Y. Sun, Y. Cui, *ACS Cent. Sci.* **2015**, *1*, 449–455.
[28] S. Liu, S. Tang, X. Zhang, A. Wang, Q. H. Yang, J. Luo, *Nano Lett.* **2017**, *17*, 5862–5868.

RESEARCH ARTICLE

Cycling more: A composite material with Na_4Si_4 and Na_2SiO_3 nanocrystals, NaSGII, was successfully used as host material for sodium deposition and dissolution in aprotic sodium metal batteries (SMBs). Improved electrokinetics of the process, stable cycling and low overpotentials are achieved, demonstrating that NaSGII has promising features for its employment in the field of SMBs.

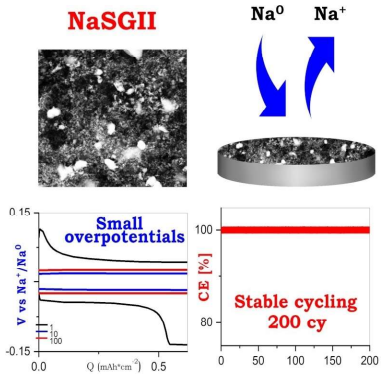

*A. Petrongari, M. Tuccillo, Dr. A. Ciccioli, Prof. A. Latini, Prof. S. Brutti**